

Breakup and fusion of ${}^6\text{Li}$ and ${}^6\text{He}$ with ${}^{208}\text{Pb}$

K. Rusek*

*Department of Nuclear Reactions, The Andrzej Soltan Institute for Nuclear Studies, Hoża, 69, 00-681 Warsaw, Poland*N. Alamanos, N. Keeley, and V. Lapoux
*DSM/DAPNIA/SPhN CEA-Saclay, 91191 Gif-sur-Yvette, France*A. Pakou
Department of Physics, The University of Ioannina, 45110 Ioannina, Greece
(Received 26 March 2004; published 8 July 2004)

The effect of ${}^6\text{Li}$ and ${}^6\text{He}$ breakup on the fusion cross section of these nuclei with ${}^{208}\text{Pb}$ is investigated by means of continuum-discretized coupled-channels (CDCC) calculations. For ${}^6\text{Li}$ the calculations describe reasonably well the experimental data for elastic scattering, ${}^6\text{Li} \rightarrow \alpha + d$ breakup and the absorption cross section given by the sum of the ${}^6\text{Li}$ fusion and the α production cross section not attributed to breakup. The effect of ${}^6\text{Li}$ breakup on the calculated absorption cross section is found to depend strongly on the imaginary part of the diagonal bare potential. A combination of the CDCC technique and the barrier penetration model generates results close to the measured fusion cross section. For ${}^6\text{He}$ the calculated absorption cross section is much larger than the measured ${}^6\text{He} + {}^{209}\text{Bi}$ complete fusion cross section values. However, it is found to be relatively independent of the form of the imaginary part of the bare potential. The complete fusion cross section is again found to be reasonably well described by the CDCC/BPM combination.

DOI: 10.1103/PhysRevC.70.014603

PACS number(s): 21.60.Gx, 24.10.Eq, 25.70.Bc, 25.70.De.

I. INTRODUCTION

The fusion probability of two colliding nuclei is sensitive to their structure as well as to the influence of other processes such as nucleon transfer or breakup. It is expected that for weakly bound projectiles breakup will be the dominant direct reaction process and due to this expectation the effect of breakup on other reaction channels, especially the fusion process, has recently been intensively investigated. Many of the fusion studies published to date lead to contradictory conclusions. Some of them predict a large enhancement of the fusion cross section below the Coulomb barrier due to breakup, while others observe a rather large suppression of the fusion cross section [1–5].

Generally, theoretical models used in these studies are based on the coupled-channels (CC) formalism. This method allows the effect of projectile breakup on fusion to be studied, since the total reaction cross section, σ_R , can be expressed as:

$$\sigma_R = \sigma_{br} + \sigma_{abs} = \frac{\pi}{K^2} \sum_l (2l+1)(1 - |S_l|^2), \quad (1)$$

where the elastic scattering S -matrix elements, S_l , and breakup cross section, σ_{br} , are directly provided by the CC calculations. Here $\hbar K$ represents the relative momentum of the two colliding nuclei in the entrance channel. If breakup is the dominant direct reaction process, the absorption cross section, σ_{abs} , is equal to the fusion cross section, σ_{fus} , as contributions to σ_{abs} from other direct reaction channels not explicitly included in the calculation may be neglected in this

case. An effective method of calculating the breakup cross section is the continuum-discretized coupled-channels (CDCC) formalism [6]. The continuum of unbound states above the breakup threshold is discretized into bins in momentum space. Each bin is then represented as an individual state in the CC formalism, using a wave function obtained by averaging the continuum wave functions calculated within that bin over its width.

A weakly bound projectile scattering system that has been well investigated experimentally is ${}^6\text{Li} + {}^{208}\text{Pb}$. The elastic scattering of ${}^6\text{Li}$ by ${}^{208}\text{Pb}$ has been measured at several energies in the vicinity of the Coulomb barrier [7,8]. The sequential breakup process ${}^6\text{Li} \rightarrow \alpha + d$ proceeding via the first resonant 3^+ state was measured at three incident energies by Gemmeke *et al.* [8], while the total inclusive and exclusive breakup was recently investigated by Signorini *et al.* [9]. Moreover, very recently Wu *et al.* [10] published cross sections for the fusion of ${}^6\text{Li}$ with ${}^{208}\text{Pb}$. These data form an almost complete set for the interaction of ${}^6\text{Li}$ with ${}^{208}\text{Pb}$.

The interaction of ${}^6\text{Li} + {}^{208}\text{Pb}$ has also been investigated theoretically by means of CDCC calculations. Results for elastic scattering and breakup were published in our earlier papers [11,12]. In a recent paper [13] we have also shown some results for the fusion of ${}^6\text{Li}$ with ${}^{208}\text{Pb}$. They were obtained using a barrier penetration model (BPM) with the real effective potential between the projectile and target being the sum of the bare potential and the dynamic polarization potential. The latter was generated by the couplings to the resonant and nonresonant excited states of ${}^6\text{Li}$ included in the CDCC calculations. The nucleus ${}^6\text{Li}$ is known to have a well developed $\alpha + d$ cluster structure, therefore the bare potential was calculated from empirical optical model $\alpha + \text{target}$ and $d + \text{target}$ potentials using the cluster wave function of the ${}^6\text{Li}$ ground state and the single-folding technique

*Electronic address: rusek@fuw.edu.pl

[14]. The results could not be compared to measured fusion cross sections as none were available at that time.

Recently Diaz-Torres *et al.* [15] proposed a novel method for calculating fusion, still based on CDCC calculations using the $\alpha+d$ cluster model of ${}^6\text{Li}$. They focused on the fusion of ${}^6\text{Li}$ with ${}^{59}\text{Co}$ and ${}^{209}\text{Bi}$ without presenting results for other reaction channels. Their CDCC calculations employed α and d +target potentials with short-ranged imaginary components to simulate an incoming wave boundary condition. However, they did not include imaginary components in the transition potentials.

The present paper is devoted to a more detailed study of breakup effects on the fusion of ${}^6\text{Li}$ and ${}^6\text{He}$. We present the results of different model calculations including CDCC calculations with different input potentials. The aim of this work is to ascertain whether modern reaction models can describe simultaneously the elastic scattering, breakup and fusion processes for the interaction of these weakly bound light nuclei with a ${}^{208}\text{Pb}$ target. We compare calculated cross sections with many existing data sets, including elastic scattering, sequential and total breakup, and fusion. We study the problem of fusion enhancement and fusion suppression and the dependence of these effects on the imaginary part of the diagonal bare potential as well as on the nature, Coulomb or nuclear, of the breakup process.

II. MODEL CALCULATIONS

A. Continuum-discretized coupled-channels

The CDCC method was used to calculate cross sections for the elastic and breakup channels. From these observables the absorption cross section was extracted by means of Eq. (1). For ${}^6\text{Li}$, couplings to the 3^+ ($E_x=2.18$ MeV), 2^+ ($E_x=4.31$ MeV) and 1^+ ($E_x=5.65$ MeV) resonant states were included as well as couplings to the nonresonant $\alpha+d$ continuum. The continuum was truncated at an excitation energy of about 11 MeV, corresponding to an $\alpha+d$ relative momentum $k=0.78$ fm $^{-1}$. The continuum was discretized into bins of equal width, $\Delta k=0.26$ fm $^{-1}$. In the presence of resonances the discretisation was slightly modified in order to avoid double counting. All cluster states corresponding to $\alpha+d$ relative angular momenta $L=0, 1, 2$ were included. The resonant states were also treated as momentum bins, with widths corresponding to 0.1 MeV, 2.0 MeV, and 3.0 MeV, respectively [16]. The $\alpha+d$ binding potential was of Woods-Saxon shape with parameters $R=1.9$ fm and $a=0.65$ fm [17]. More details concerning the parameters used in the present CDCC calculations can be found in Refs. [11,12,18].

The diagonal and coupling interactions were calculated from α +target and d +target optical model potentials by means of the single-folding technique [14]. Two sets of input potentials were used. Set A consisted of empirical $\alpha+{}^{208}\text{Pb}$ and $d+{}^{208}\text{Pb}$ optical potentials obtained in low energy elastic scattering studies [19,20], and calculations with this set are referred to as CDCC A. In order to investigate the sensitivity of the results to the bare imaginary potential, we also performed calculations where the imaginary parts of the $\alpha, d+{}^{208}\text{Pb}$ optical model potentials were replaced by a short-ranged potential with parameters $W=50$ MeV, $r_i=1.0$ fm,

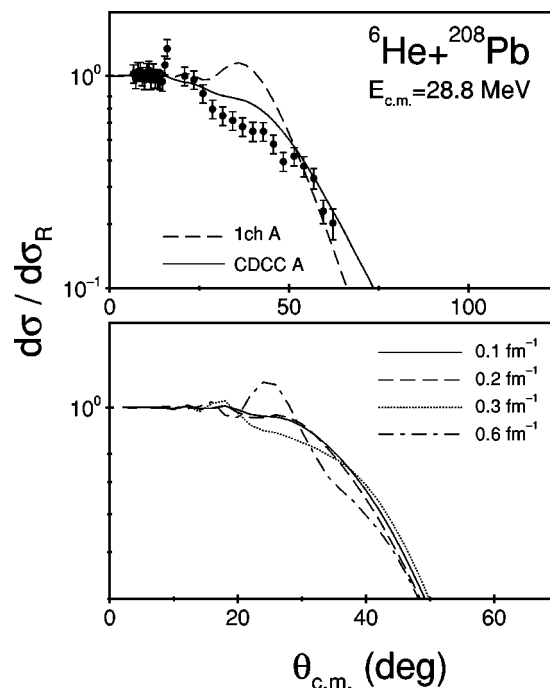


FIG. 1. (a) Angular distribution of the differential cross section (ratio to Rutherford cross section) for ${}^6\text{He}+{}^{208}\text{Pb}$ elastic scattering [13]. The curves show results of one-channel and the full CDCC calculations with the set A of the input cluster-target potentials. (b) Results of the CDCC test calculations with different width of the continuum bins. See text for details.

and $a_i=0.2$ fm, in order to simulate an in-going-wave boundary condition for fusion, following the prescription of Rhoades-Brown and Braun-Munzinger [21]. CDCC calculations using these parameters are referred to as CDCC B.

The binding energy of ${}^6\text{He}$ is even smaller than that of ${}^6\text{Li}$, so breakup is expected to be more dominant in the interaction of ${}^6\text{He}$ with a target nucleus and to have a much larger effect on the fusion process. Also, ${}^6\text{He}$ has a strong $E1$ excitation to the continuum, whereas in a strict $\alpha+d$ cluster model of ${}^6\text{Li}$ the $E1$ excitation strength is identically equal to zero [22]. Therefore, we performed similar CDCC calculations for the ${}^6\text{He}+{}^{208}\text{Pb}$ scattering system, using a two-body dineutron model of ${}^6\text{He}$ [13,23]. Although ${}^6\text{He}$ is known to have a three-body $\alpha+n+n$ structure there are reasonable grounds for believing that the dineutron model generates physically meaningful results. As discussed in Keeley *et al.* [22] the dineutron model of ${}^6\text{He}$ produces $E1$ coupling strengths that exhaust similar amounts of both the Thomas-Reiche-Kuhn and cluster energy weighted sum rules to the values extracted experimentally by Aumann *et al.* [24]. The dineutron model $E1$ strength is thus not unreasonable. In the calculations couplings to the 1.8 MeV 2^+ resonant state of ${}^6\text{He}$ and to the $L=0, 1, 2$ nonresonant continuum, truncated at an excitation energy of about 12.3 MeV, corresponding to an $\alpha+{}^2n$ relative momentum $k=0.85$ fm $^{-1}$, were included. The continuum was discretised into bins of width $\Delta k=0.25$ fm $^{-1}$ for the lowest energy bins for each L value and $\Delta k=0.20$ fm $^{-1}$ for the others. The results for the elastic scattering are compared to the experimental data in Fig. 1(a). Test calculations with the model space limited to the $L=1$

states from the continuum and with the different bin widths are presented in Fig. 1(b). In the calculations the continuum was truncated at $k=0.85\text{ fm}^{-1}$. It was found that the calculations with the $\Delta k=0.20\text{ fm}^{-1}$ generate very similar results to the calculations with the $\Delta k=0.10\text{ fm}^{-1}$. Values of the breakup cross section calculated with these two bin widths differ by less than 1%. As input cluster-target potentials we adopted the two sets used in the ${}^6\text{Li}+{}^{208}\text{Pb}$ calculations.

B. Barrier penetration model

In the limit of no couplings, optical model calculations of the absorption cross section with short ranged imaginary potentials should give results close to the fusion cross section calculated using the barrier penetration model (BPM). In the BPM the fusion cross section is calculated from the barrier penetration coefficients, T_l , using the following relation:

$$\sigma_{\text{fus}} = \frac{\pi}{K^2} \sum_l (2l+1) T_l. \quad (2)$$

The coefficients T_l in turn are calculated using the WKB approximation and they depend on the Coulomb barrier, $U_B = U_{\text{nuclear}}^{\text{real}} + U_{\text{coulomb}}$. For the optical model case, when the imaginary part of the diagonal nuclear potential, U_{nuclear} , is confined inside the Coulomb barrier the values of $(1-|S_l|^2)$ obtained from Eq. (1) should be close to the BPM T_l [21,25]. Hence the BPM fusion cross section and the optical model absorption cross section will be similar for calculations with the same real part of U_{nuclear} . It was shown that when the real part of U_{nuclear} is energy dependent according to the dispersion relation, BPM calculations of the fusion cross section well reproduce the experimental data for ${}^{16}\text{O}$ fusion with ${}^{208}\text{Pb}$ and ${}^{32}\text{S}$ fusion with ${}^{40}\text{Ca}$ [26].

It is possible to account for the effect of channel couplings in one-channel calculations by means of a dynamic polarization potential, U_p . Such a potential may be derived from CDCC calculations following the prescription of Thompson *et al.* [27]. Recently, it was shown that BPM calculations with an effective nuclear potential equal to the sum of the bare potential and the polarization potential, $U_{\text{nuclear}} = U_{\text{eff}} = U_{\text{bare}} + U_p$, are able to describe well the cross sections for ${}^6,7\text{Li}$ fusion with ${}^{16}\text{O}$ [28,29]. In this paper we also present results of such calculations for both scattering systems.

Most of the calculations presented in this paper were performed using the code Fresco [31], version frxp18.

III. RESULTS AND DISCUSSION

A. Results for ${}^6\text{Li}+{}^{208}\text{Pb}$

A typical example of the description of an elastic scattering angular distribution by the CDCC calculations is shown in Fig. 2. Calculations with the empirical cluster-target optical model potentials (CDCC A) describe the data better than those with the short-ranged imaginary parts (CDCC B). This is due to the empirical potentials having more surface absorption, which in a broad sense models the effect of target

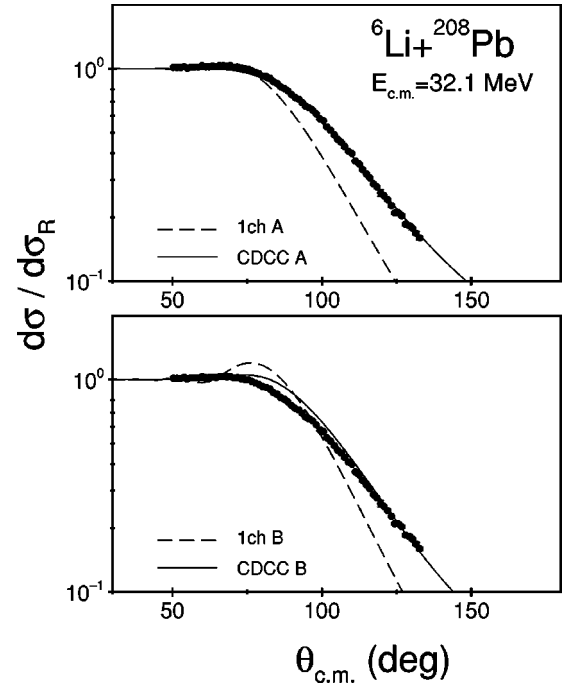


FIG. 2. Angular distribution of the differential cross section (ratio to Rutherford cross section) for ${}^6\text{Li}+{}^{208}\text{Pb}$ elastic scattering. The data are from Keeley *et al.* [7]. The curves show results of various calculations with the two sets, A and B, of input cluster-target potentials. One-channel no coupling calculations are plotted as dashed curves while the calculations with ${}^6\text{Li} \rightarrow \alpha+d$ breakup couplings included are plotted as solid curves, see text for details.

inelastic excitations and other channels not explicitly included in the calculations. The effect of breakup on the elastic channel is shown by the difference between the one-channel calculations (dashed curves) and the full CDCC results (solid curves). Here the one-channel calculations are equivalent to the optical model calculations with the complex potential derived from cluster-target empirical interactions by means of single-folding technique.

The dynamic polarization potential derived from the CDCC A calculations reduces the strength of the bare potential at the Coulomb barrier radius. This reduction varies slightly with incident energy (see Table I) and is different for the real and imaginary parts. The mean value of this reduction is $N_r=0.57$ and $N_i=0.90$ for the real and imaginary parts of the potential, respectively, indicating that the polarization potential is mostly real and repulsive at the surface for these calculations.

TABLE I. Ratios of the real (N_r) and imaginary (N_i) parts of $U_{\text{eff}}/U_{\text{bare}}$ at the Coulomb barrier radius ($R_C=11.6\text{ fm}$) for ${}^6\text{Li}+{}^{208}\text{Pb}$ extracted from the CDCC A calculations.

$E_{\text{c.m.}}$	N_r	N_i
26.6	0.61	1.12
28.2	0.52	0.99
32.0	0.52	0.80
37.9	0.58	0.78
50.5	0.63	0.79

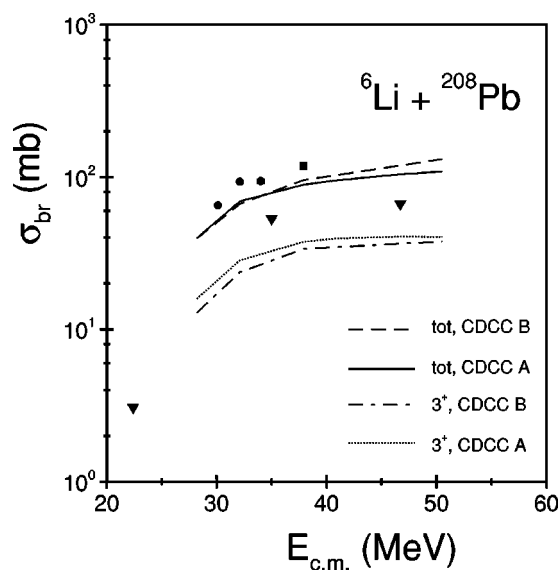


FIG. 3. Data for the exclusive ${}^6\text{Li}$ breakup from $\alpha+d$ and $\alpha+p$ coincidences measured by Signorini *et al.* [9] (filled circles) and for the sequential ${}^6\text{Li} \rightarrow \alpha+d$ breakup via the 3^+ resonant state of ${}^6\text{Li}$ obtained by Gemmeke *et al.* [8] (triangles) compared with the CDCC calculations. See text for details.

The results for the ${}^6\text{Li} \rightarrow \alpha+d$ breakup cross section do not depend so strongly on the choice of input imaginary potential parameters. For sequential breakup via the 3^+ resonant state of ${}^6\text{Li}$ both sets of calculations (CDCC A and CDCC B) underpredict the cross section, but for the total breakup (the sum of the sequential and direct breakup) the agreement is better. The filled circles in Fig. 3 denote the experimental values for the cross sections corresponding to the sum of the exclusive $\alpha+d$ and $\alpha+p$ coincidences, so in addition to the ${}^6\text{Li} \rightarrow \alpha+d$ breakup they include contributions from the one-neutron transfer process and from the three-body $\alpha+p+n$ direct breakup. Test calculations have shown that one-neutron transfer to the first few excited states of ${}^{209}\text{Pb}$ generates a total cross section of about the same size as that for breakup. Couplings to these transfer channels were not included in the present calculations, so the predicted cross section values should be lower than the measured ones.

The absorption cross sections obtained from the CDCC calculations are presented in Fig. 4(a). They are plotted as a function of the c.m. energy (ratio to the Coulomb barrier height, V_B). The height of the Coulomb barrier was found to be 28.5 MeV at a ${}^6\text{Li}+{}^{208}\text{Pb}$ separation of $R_C=11.6$ fm in the cluster-folding calculations. For weakly bound projectiles like ${}^6\text{Li}$, one should distinguish between *complete* and *total* fusion [2]. The latter contains, in addition to the fusion of the projectile as a whole with the target (complete fusion), fusion of one or more projectile fragments with the target. The absorption cross sections obtained from the CDCC calculations correspond to total fusion, since the imaginary parts of the cluster-target input potentials account for the separate fusion of the α and d with ${}^{208}\text{Pb}$. The problem of complete versus total fusion and the various definitions of these quantities found in the literature is extensively discussed in Diaz-Torres *et al.* [15].

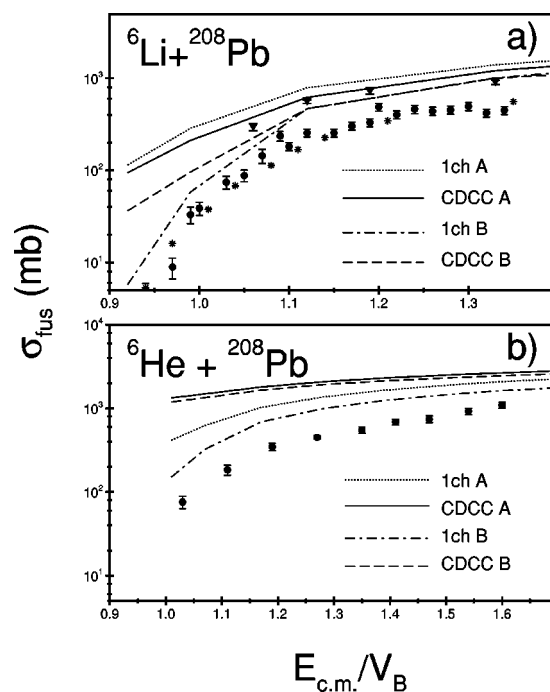


FIG. 4. (a) Experimental data for ${}^6\text{Li}+{}^{208}\text{Pb}$ (filled circles) [10] and ${}^6\text{Li}+{}^{209}\text{Bi}$ fusion (stars) [2] compared to the absorption cross sections obtained from the CDCC A and CDCC B calculations. The filled triangles represent the sum of the fusion cross section and the so called *stripping breakup*, the difference between the total α production cross section and the exclusive breakup cross section as discussed in Ref. [9]. (b) Experimental data for the ${}^6\text{He}+{}^{209}\text{Bi}$ complete fusion cross section (filled circles) [4] compared with the absorption cross sections obtained from the CDCC A and CDCC B calculations for ${}^{208}\text{Pb}$ target.

The calculated cross sections are compared with the experimental results of Wu *et al.* [10] for ${}^6\text{Li}+{}^{208}\text{Pb}$ fusion, plotted by the solid circles in Fig. 4(a). As expected, the one-channel calculations with input potential set A (dotted curve) generate larger cross sections than those using set B (dotted-dashed curve). This is simply because the imaginary part of the diagonal potential derived from set A is of larger range than that derived from set B. In both cases, however, the absorption cross sections obtained from the full CDCC calculations are much larger than the experimental fusion cross sections. This is not surprising, as the experimental values represent mainly complete fusion of ${}^6\text{Li}$ with ${}^{208}\text{Pb}$.

The calculated values of the absorption cross section are close, however, to the sum of the fusion cross section and the so called *stripping breakup* cross section, $\sigma_{\text{str.BU}}$, measured by Signorini *et al.* [9] (solid triangles). The latter is the difference between the total α production cross section seen in the experiment and the exclusive breakup cross section plotted in Fig. 3. Both calculations, CDCC A and CDCC B, produce similar quality fits to these data.

The effect of breakup on the absorption cross section is very different, depending on the input parameter set. For set A breakup reduces the absorption cross section over the whole energy range (solid curve), while for set B, the absorption cross section remains almost unchanged above the Coulomb barrier and is significantly enhanced below the barrier

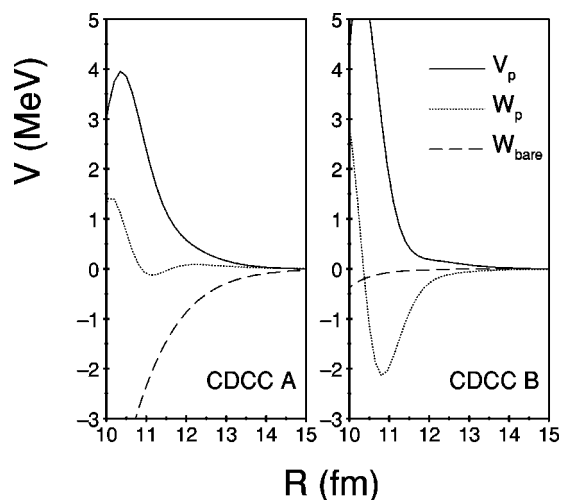


FIG. 5. Real (V_p) and imaginary (W_p) parts of the dynamic polarization potential (U_p) corresponding to the two different CDCC calculations at $E_{c.m.} = 28.2$ MeV for ${}^6\text{Li} + {}^{208}\text{Pb} \rightarrow (\alpha + d) + {}^{208}\text{Pb}$ breakup. The imaginary parts of the respective ${}^6\text{Li} + {}^{208}\text{Pb}$ bare potentials (U_{bare}) are plotted by the dashed curves.

(dashed curve). It is important to note that the calculated values of the absorption cross section, independent of the input potential set, are close to the experimental values $\sigma_{\text{fus}} + \sigma_{\text{str.BU}}$ plotted by the solid triangles.

The effect of the breakup process on the fusion cross section may be discussed in terms of the dynamic polarization potential. It is well known that the effect of ${}^6\text{Li}$ breakup on the elastic scattering cross section may be simulated in a one-channel calculation by a polarization potential with a repulsive real part. Ioannides and Mackintosh [32] have noted that this “*repulsion tends to occur more strongly when the underlying absorption is strongest.*” Sakuragi [30] studied the real and imaginary parts of the dynamic polarization potential generated by ${}^6\text{Li}$ breakup and found that the ratio of these two terms depends on the nature of the coupling potentials. When purely real coupling potentials are used in CDCC calculations the dynamic polarization potential has a significant absorptive imaginary part, but when complex coupling potentials are used the imaginary part of the polarization potential is negligibly small at the surface.

These observations correspond directly to the polarization potentials derived from our calculations using the two sets of input potentials. In Fig. 5 the real and imaginary parts of the polarization potentials derived from the CDCC A and CDCC B calculations at a c.m. energy of 28.2 MeV are plotted together with the respective imaginary part of the diagonal potential, W_{bare} . When set A is used, the derived polarization potential has a negligibly small imaginary part at separations larger than the Coulomb barrier radius, while when set B is used the imaginary part of the polarization potential becomes strongly absorptive around the barrier radius. Thus, in the CDCC A calculations the absorption cross section is mainly determined by the lowering of the Coulomb barrier due to the repulsive real polarization potential, while in the CDCC B calculations the absorption generated at the surface is responsible for the increase of the absorption cross section below the barrier.

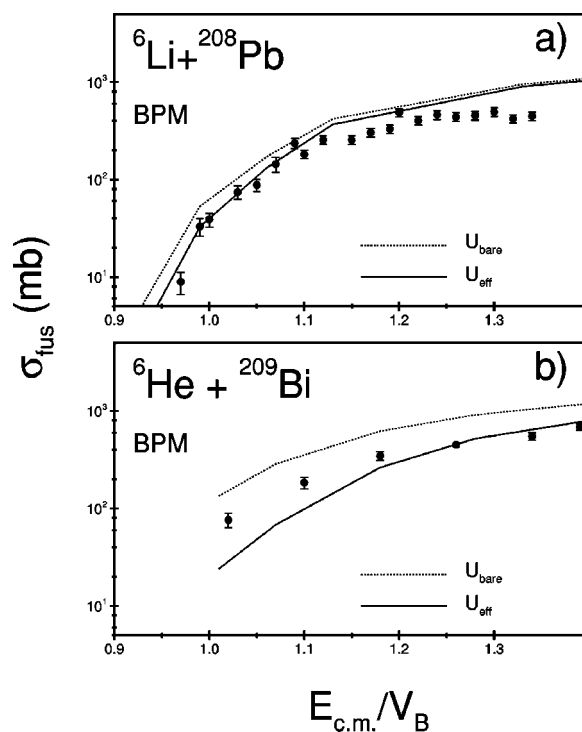


FIG. 6. (a) Fusion cross sections for ${}^6\text{Li} + {}^{208}\text{Pb}$ (filled circles) [10] plotted as a function of the c.m. energy (ratio to the Coulomb barrier height). The curves show the results of calculations using a combination of CDCC and BPM techniques with the bare and effective potentials. See text for details. (b) Fusion cross sections for ${}^6\text{He} + {}^{209}\text{Bi}$ (filled circles) [4]. The curves show the results of calculations using a combination of CDCC and BPM techniques with the bare and effective potentials. See text for details.

A comparison of the cross sections for fusion of ${}^6\text{Li}$ with ${}^{208}\text{Pb}$ (solid circles) and ${}^{209}\text{Bi}$ (stars) plotted in Fig. 4(a) suggests that target excitation plays a negligible role in the fusion process. This is supported by test CDCC calculations which included coupling to the 2.6 MeV 3_1^- excited state of ${}^{208}\text{Pb}$.

Calculations of the fusion cross section using the BPM/CDCC model depend only very weakly on the input parameters sets A, B since in this model the fusion cross section is mainly defined by the real part of the effective nuclear potential, $U_{\text{nuclear}} = U_{\text{eff}}$. Therefore, in Fig. 6(a) we only show the results of BPM calculations using input potential parameter set A. The results of the calculations with the diagonal nuclear potential equal to the bare potential, $U_{\text{nuclear}} = U_{\text{bare}}$, are shown by the dotted curve. When the polarization potential is added to the bare potential the fusion cross section is slightly suppressed below the Coulomb barrier (solid curve).

B. Results for ${}^6\text{He} + {}^{208}\text{Pb}$

The mechanisms of ${}^6\text{Li} \rightarrow \alpha + d$ and ${}^6\text{He} \rightarrow \alpha + 2n$ breakup in the field of a lead target are very different [13,33]. Breakup of ${}^6\text{Li}$ is governed by the nuclear interaction while breakup of ${}^6\text{He}$ is dominated by Coulomb couplings to the continuum. Verbitskiĭ and Terenetskiĭ [34] demonstrated that if ${}^6\text{He}$ breakup is of Coulomb nature the dynamic polariza-

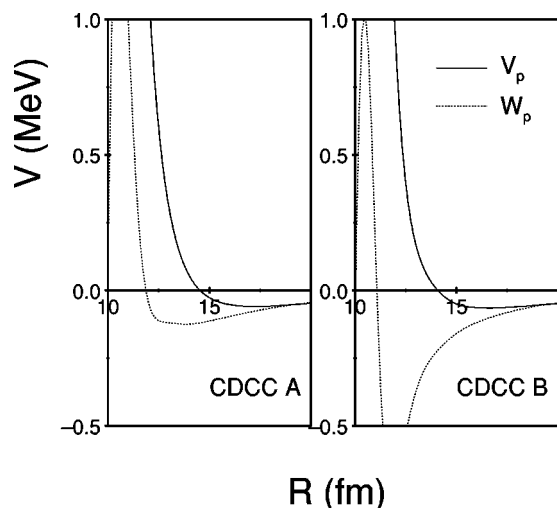


FIG. 7. Dynamic polarization potentials corresponding to the two different CDCC calculations as in Fig. 5 but for ${}^6\text{He}+{}^{208}\text{Pb}$ at $E_{\text{c.m.}}=28.8$ MeV.

tion potential corresponding to this process has a small attractive real part and a much stronger absorptive imaginary part of a very long range.

This observation is fully supported by the present CDCC calculations. Although at projectile-target separations around the Coulomb barrier radius ($R_C=12$ fm) the polarization potential still has a strong repulsive real part, it becomes small and attractive at separations larger than 14 fm, see Fig. 7. The imaginary part is already absorptive at 12 fm and dominates at separations larger than 14 fm. Thus, independent of the input potential set, the absorption cross section is defined by the long-range absorption at the surface and the absorption cross section predicted by the CDCC calculations is therefore enhanced over the whole energy range.

The results of the CDCC calculations are plotted in Fig. 4(b). As fusion data for ${}^6\text{He}+{}^{208}\text{Pb}$ are not available, the calculations are compared to measured cross sections for ${}^6\text{He}+{}^{209}\text{Bi}$ complete fusion [4]. The ${}^6\text{Li}$ fusion data were found to be similar for both targets, therefore the assumption that they are similar for ${}^6\text{He}$ is reasonable. The calculated and measured cross sections are plotted as a function of the c.m. energy, ratio to the Coulomb barrier height. The value of the Coulomb barrier height was found to be 18.2 MeV at $R_C=12$ fm for ${}^6\text{He}+{}^{208}\text{Pb}$. For the bismuth target the barrier was assumed to be slightly larger and equal to 18.4 MeV. As for ${}^6\text{Li}$, the one-channel calculations with set A (dotted curve) give much larger absorption cross sections than the calculations with input potential set B (dotted-dashed curve), as expected. However, when the couplings to the 2^+ resonance and the nonresonant continuum are included the calculated absorption becomes very similar in both cases and much larger than the measured complete fusion cross section (solid and dashed curves). One should bear in mind that the calculated absorption cross section corresponds to the total fusion and, as was shown for ${}^6\text{Li}$, includes the effect of contributions from direct reaction channels other than breakup. However, in contrast to the results for ${}^6\text{Li}+{}^{208}\text{Pb}$, we may draw the firm conclusion that the effect of ${}^6\text{He}\rightarrow{}^2n+\alpha$

breakup on the calculated absorption cross section (the “total fusion”) is a considerable enhancement, irrespective of the choice of diagonal imaginary potential.

When plotted as a function of the $E_{\text{c.m.}}/V_B$ ratio the values for the ${}^6\text{He}+{}^{209}\text{Bi}$ fusion cross section become very similar to those for fusion of ${}^6\text{Li}$ with ${}^{208}\text{Pb}$, cf. Figs. 6(a) and 6(b). The description of the experimental fusion cross sections by the BPM calculations is shown by the solid curve in Fig. 6(b). These calculations reflect the enhancement of the Coulomb barrier due to the repulsive real part of the polarization potential at the barrier, and therefore the effect of ${}^6\text{He}$ breakup on the fusion cross section predicted by the BPM calculations is opposite to that obtained from the full CDCC calculations. The BPM predicts strong suppression of the fusion cross section due to breakup, as a comparison of the solid and dotted curves in Fig 6(b) shows. The large difference between the full CDCC and BPM results can be due to other than breakup reaction channels not taken into account in the CDCC calculations.

IV. CONCLUSIONS

Results of extensive CDCC calculations for the interaction of ${}^6\text{Li}$ and ${}^6\text{He}$ with a ${}^{208}\text{Pb}$ target have been presented. The calculations are able to describe data for ${}^6\text{Li}+{}^{208}\text{Pb}$ elastic scattering, ${}^6\text{Li}\rightarrow\alpha+d$ breakup and “nonbreakup absorption” reasonably well. The latter observable is the sum of the ${}^6\text{Li}+{}^{208}\text{Pb}$ fusion and the so called stripping breakup, the process which is responsible for 75% of the measured α particle yield for the ${}^6\text{Li}+{}^{208}\text{Pb}$ interaction. The mechanism of this process remains to be elucidated and its effect on fusion needs to be further investigated.

The effect of the ${}^6\text{Li}\rightarrow\alpha+d$ breakup on the calculated absorption cross section is found to depend strongly on the nature of the imaginary part of the diagonal bare potential. If the imaginary bare potential is weak at the surface (CDCC B calculations), the inclusion of breakup enhances the calculated absorption cross section below the Coulomb barrier, leaving it unchanged above the barrier. If the imaginary bare potential is strong in the surface (CDCC A calculations), breakup reduces the calculated absorption cross section over the whole energy range. However, both sets of calculations give similar final results for the absorption cross section, in broad agreement with the experimental “nonbreakup absorption” cross sections.

The CDCC/BPM calculations provide a reasonable description of the *complete* fusion data, and predict general suppression of the fusion cross section due to breakup below the Coulomb barrier.

The absorption cross section values for ${}^6\text{He}+{}^{208}\text{Pb}$ obtained from the full CDCC calculations are much larger than the measured complete fusion cross sections for the bismuth target. Both sets of CDCC calculations predict strong enhancement of the absorption cross section over the whole energy range and give essentially identical final results, independent of the nature of the bare imaginary potential. This insensitivity to the choice of diagonal imaginary potential may be ascribed to the dominant nature of Coulomb breakup for ${}^6\text{He}$, in contrast to ${}^6\text{Li}$.

As for ${}^6\text{Li}+{}^{208}\text{Pb}$, the CDCC/BPM calculations give a reasonably good account of the complete fusion cross sections and predict a general suppression of the fusion cross section due to breakup, the effect being considerably more important for ${}^6\text{He}$.

The large difference between the CDCC absorption cross sections and the measured complete fusion cross sections shows that a full understanding of the fusion process is not possible without a simultaneous understanding of other reaction channels which proceed with large cross sections, such as transfer processes, and calls for more detailed experimental and computational studies. However, our results do lead to the conclusion that the CDCC absorption cross section is not the appropriate theoretical quantity to compare with complete fusion, but rather with the *total* fusion. This conclusion is also physically reasonable, as the calculated absorption cross section is the sum of absorption by the imaginary potentials out of all channels, including those for which the ${}^6\text{He}$ or ${}^6\text{Li}$ is no longer bound.

Summarizing, we have shown that for both scattering systems the absorption cross section obtained from Eq. (1) with the breakup cross section calculated by means of the CDCC

method is much larger than the experimental *complete* fusion cross sections. CDCC calculations using an interior imaginary potential suggest that the effect of breakup on the absorption cross section is enhancement below the barrier with little or no change above it for ${}^6\text{Li}$ and a general enhancement for ${}^6\text{He}$. The *complete* fusion cross section appears to be rather well described by a combination of the CDCC and BPM methods, these calculations indicating a suppression of the sub-barrier complete fusion cross section by the breakup couplings. These results provide an *a posteriori* justification of the general scheme used to calculate sub-barrier fusion in Ref. [1].

ACKNOWLEDGMENTS

The authors thank Professor J. J. Kolata, Dr. M. Dasgupta, and Dr. Y. W. Wu for providing numerical values of the fusion cross section data discussed in this paper. This work was financially supported by the State Committee for Scientific Research of Poland (KBN), Grant No. POLONIUM 4335.II/2003.

-
- [1] N. Alamanos, A. Pakou, V. Lapoux, J. L. Sida, and M. Trotta, Phys. Rev. C **65**, 054606 (2002).
- [2] M. Dasgupta, D. J. Hinde, K. Hagino, S. B. Moraes, P. R.S. Gomes, R. M. Anjos, R. D. Butt, A. C. Berriman, N. Carlin, C. R. Morton, J. O. Newton, and A. Szanto de Toledo, Phys. Rev. C **66**, 041602 (2002).
- [3] C. H. Dasso and A. Vitturi, Phys. Rev. C **50**, R12 (1994).
- [4] J. J. Kolata, V. Guimaraes, D. Peterson, P. Santi, R. White-Stevens, P. A. DeYoung, G. F. Peaslee, B. Hughey, B. Atalla, M. Kern, P. L. Jolivet, J. A. Zimmerman, M. Y. Lee, F. D. Becchetti, E. F. Aguilera, E. Martinez-Quiroz, and J. D. Hinnfeld, Phys. Rev. Lett. **81**, 4580 (1998).
- [5] M. Trotta, J. L. Sida, N. Alamanos, A. Andreyev, F. Auger, D. L. Balabanski, C. Borcea, N. Coulier, A. Drouart, D. J.C. Durand, G. Georgiev, A. Gillibert, J. D. Hinnfeld, M. Huysse, C. Jouanne, V. Lapoux, A. Lépine, A. Lumbroso, F. Marie, A. Musumarra, G. Neyens, S. Ottini, R. Raabe, S. Ternier, P. Van Duppen, K. Vyvey, C. Volant, and R. Wolski, Phys. Rev. Lett. **84**, 2342 (2000).
- [6] N. Austern, Y. Iseri, M. Kamimura, M. Kawai, G. Rawitscher, and M. Yahiro, Phys. Rep. **154**, 125 (1987).
- [7] N. Keeley, S. J. Bennett, N. M. Clarke, B. R. Fulton, G. Tungate, P. V. Drumm, M. A. Nagarajan, and J. S. Lilley, Nucl. Phys. **A571**, 326 (1994).
- [8] H. Gemmeke, B. Deluigi, L. Lassen, and D. Scholz, Z. Phys. A **286**, 73 (1978).
- [9] C. Signorini, A. Edifizi, M. Mazzocco, M. Lunardon, D. Fabris, A. Vitturi, P. Scopel, F. Soramel, L. Stroe, G. Prete, E. Fioretto, M. Cinausero, M. Trotta, A. Brondi, R. Moro, G. La Rana, E. Vardaci, A. Ordine, G. Inghima, M. La Commara, D. Pierrousakou, M. Romoli, M. Sandoli, A. Diaz-Torres, I. J. Thompson, and Z. H. Liu, Phys. Rev. C **67**, 044607 (2003).
- [10] Y. W. Wu, Z. H. Liu, C. J. Lin, H. Q. Zhang, M. Ruan, F. Yang, Z. C. Li, M. Trotta, and K. Hagino, Phys. Rev. C **68**, 044605 (2003).
- [11] N. Keeley and K. Rusek, Phys. Lett. B **375**, 9 (1996).
- [12] G. R. Kelly, N. J. Davis, R. P. Ward, B. R. Fulton, G. Tungate, N. Keeley, K. Rusek, E. E. Bartosz, P. D. Cathers, D. D. Caussyn, T. L. Drummer, and K. W. Kemper, Phys. Rev. C **63**, 024601 (2001).
- [13] K. Rusek, N. Keeley, K. W. Kemper, and R. Raabe, Phys. Rev. C **67**, 041604 (2003).
- [14] B. Buck and A. A. Pilt, Nucl. Phys. **A280**, 133 (1977).
- [15] A. Diaz-Torres, I. J. Thompson, and C. Beck, Phys. Rev. C **68**, 044607 (2003).
- [16] N. Keeley and K. Rusek, Phys. Lett. B **427**, 1 (1998).
- [17] K.-I. Kubo and M. Hirata, Nucl. Phys. **A187**, 186 (1972).
- [18] K. Rusek, N. M. Clarke, and R. P. Ward, Phys. Rev. C **50**, 2010 (1994).
- [19] C. M. Perey and F. G. Perey, Phys. Rev. **132**, 755 (1963).
- [20] G. Goldring, M. Samuel, B. A. Watson, M. C. Bertin, and S. L. Tabor, Phys. Lett. **32B**, 465 (1970).
- [21] M. J. Rhoades-Brown and P. Braun-Munzinger, Phys. Lett. **136B**, 19 (1984).
- [22] N. Keeley, J. M. Cook, K. W. Kemper, B. T. Roeder, W. D. Weintraub, F. Maréchal, and K. Rusek, Phys. Rev. C **68**, 054601 (2003).
- [23] K. Rusek, K. W. Kemper, and R. Wolski, Phys. Rev. C **64**, 044602 (2001).
- [24] T. Aumann, D. Aleksandrov, L. Axelsson, T. Baumann, M. J.G. Borge, L. V. Chulkov, J. Cub, W. Dostal, B. Eberlein, Th. W. Elze, H. Emling, H. Geissel, V. Z. Goldberg, M. Golovkov, A. Grünschloss, M. Hellström, K. Hencken, J. Holeczek, R. Holzmann, B. Jonson, A. A. Korshenninikov, J. V. Kratz, G. Kraus, R. Kulesa, Y. Leifels, A. Leistenschneider, T. Leth, I. Mukha, G. Münzenberg, F. Nickel, T. Nilsson, G. Nyman, B.

- Petersen, M. Pfützner, A. Richter, K. Riisager, C. Scheidenberger, G. Schrieder, W. Schwab, H. Simon, M. H. Smedberg, M. Steiner, J. Stroth, A. Surowiec, T. Suzuki, O. Tengblad, and M. V. Zhukov, *Phys. Rev. C* **59**, 1252 (1999).
- [25] M. J. Rhoades-Brown and M. Prakash, *Phys. Rev. Lett.* **53**, 333 (1984).
- [26] C. Mahaux, H. Ngô, and G. R. Satchler, *Nucl. Phys.* **A449**, 354 (1986).
- [27] I. J. Thompson, M. A. Nagarajan, J. S. Lilley, and M. J. Smithson, *Nucl. Phys.* **A505**, 84 (1989).
- [28] N. Keeley, K. W. Kemper, and K. Rusek, *Phys. Rev. C* **65**, 014601 (2001).
- [29] M. Ray, A. Mukherjee, M. Saha Sarkar, A. Goswami, S. Roy, S. Saha, R. Bhattacharya, B. R. Behera, S. K. Datta, and B. Dasmahapatra, *Phys. Rev. C* **68**, 067601 (2003).
- [30] Y. Sakuragi, *Phys. Rev. C* **35**, 2161 (1987).
- [31] I. J. Thompson, *Comput. Phys. Rep.* **7**, 167 (1988).
- [32] A. A. Ioannides and R. S. Mackintosh, *Phys. Lett.* **161B**, 43 (1985).
- [33] A. Pakou, N. Alamanos, A. Gillibert, M. Kokkoris, S. Kossionides, A. Lagoyannis, N. G. Nicolis, C. Papachristodoulou, D. Patiris, D. Pierroutsakou, E. C. Pollacco, and K. Rusek, *Phys. Rev. Lett.* **90**, 202701 (2003).
- [34] V. P. Verbitskiĭ and K. O. Terenetskiĭ, *Sov. J. Nucl. Phys.* **55**, 198 (1992).